Photochemical & Photobiological Sciences
https://doi.org/10.1007/s43630-021-00165-0

ORIGINAL PAPERS

Excited state dynamics of Zn–salophen complexes

Patrick O'Keeffe[1] · Daniele Catone[2] · Stefano Turchini[2] · Alessandra Paladini[1] · Antonella Dalla Cort[3] · Enrico Bodo[3] · Susanna Piccirillo[2,4]

Received: 4 October 2021 / Accepted: 27 December 2021

Abstract

Zn–salophen complexes are a promising class of fluorescent chemosensors for nucleotides and nucleic acids. We have investigated, by means of steady state UV–Vis, ultrafast transient absorption, fluorescence emission and time dependent density functional theory (TD-DFT) the behavior of the excited states of a salicylidene tetradentate Schiff base (Sal), its Zn(II) coordination compound (Zn–Sal) and the effect of the interaction between Zn–Sal and adenosine diphosphate (ADP). TD-DFT shows that the deactivation of the excited state of Sal occurs through torsional motion, due to its rotatable bonds and twistable angles. Complexation with Zn(II) causes rigidity so that the geometry changes in the excited states with respect to the ground state structure are minimal. By addition of ADP to a freshly prepared Zn–Sal ethanol solution, a longer relaxation constant, in comparison to Zn–Sal, was measured, indicative of the interaction between Zn–Sal and ADP. After a few days, the Zn–Sal–ADP solution displayed the same static and dynamic behavior of a solution containing only the Sal ligand, demonstrating that the coordination of the ADP anion to Zn(II)leads to the demetallation of the Sal ligand. Fluorescence measurements also revealed an enhanced fluorescence at 375 nm following the addition of ADP to the solution, caused by the presence of 2,3-diamino naphthalene that is formed by demetallation and partial decomposition of the Sal ligand. The efficient fluorescence of this species at 375 nm could be selectively detected and used as a probe for the detection of ADP in solution.

Graphical abstract

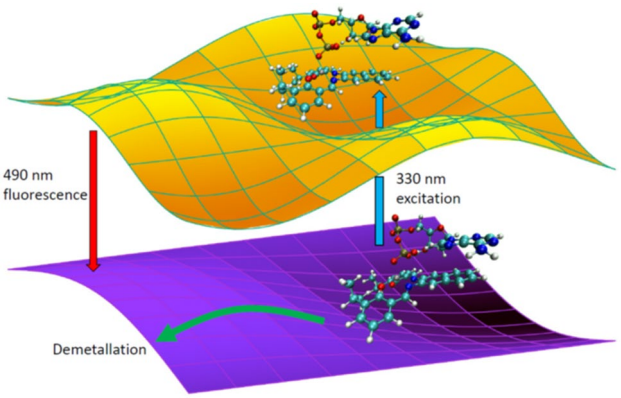

Keywords Zinc · Salophen · Adenosine diphosphate · Ultrafast transient absorption · Fluorescence emission · Time dependent density functional theory

1 Introduction

Salophens (N,N-bis(salicylidene)phenylenediamine) are tetradentate ligands, an example of which is shown in Fig. 1a, and are extensively used in coordination

✉ Susanna Piccirillo
piccirillo@fisica.uniroma2.it

Extended author information available on the last page of the article

Published online: 28 January 2022

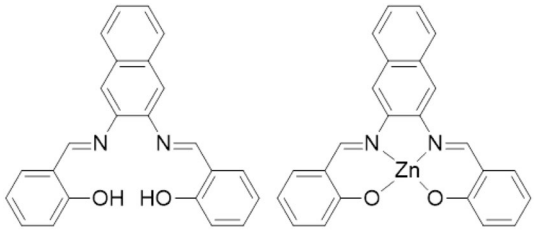

Fig. 1 Chemical formulae of the **a** salophen (Sal) and **b** Zn–salophen (Zn–Sal) compounds discussed in the text

chemistry [1, 2]. The salophen compound has two phenolic hydroxyl groups, which, following deprotonation, can form complexes with many transition and main group metals, with different oxidation states, coordination numbers and geometries that have shown interesting applications, and have been widely reported in recent literature [3–6].The catalytic, optical, electrical and biological properties of the salophen and their metal complexes can be tuned by structural modifications of the salophen unit or by changing the coordination of the metal. This versatility has encouraged extensive research in the last decade on their synthesis and characterization [7, 8].

In particular, Zn–salophen complexes often display interesting photochemical and photophysical properties [8–10]. Their ability to function as luminescent materials also makes them promising candidates for the realization of supramolecular sensors, switches, and memory devices. Due to the strong preference of Zn(II) for pentacoordination, tetracoordinated Zn–salophen complexes can easily add a monodentate ligand such as a solvent molecule or analyte. Either in solution or in the solid state they can also form aggregates where the pentacoordination of Zn(II) results from an additional bond with an oxygen atom of a second salophen unit [8, 9, 11, 12].

In previous studies [13, 14], we have initiated a structural characterization of host–guest complexes formed by specific Zn–salophen complexes, which are known to be good receptors for anions [15, 16], and often show optical sensing properties for anion recognition [17, 18]. Among them, the Zn–salophen compound shown in Fig. 1b, which we denote as Zn–Sal in the following, can efficiently bind to inorganic phosphate, and adenosine monophosphate (AMP) nucleotide anions [13]. We also reported, in a less recent study [17], that the interaction with AMP, adenosine di- or triphosphate nucleotides in solution produces significant changes in the spectral properties of this fluorophore. Specifically, the addition of nucleotides caused a 90–95% quenching of the green–yellow fluorescence of Zn–Sal, so that the latter is an on–off sensor for specific detection of these nucleotides.

We tentatively attributed this effect to the existence of stacking interactions between the aromatic rings of the Zn–salophen sensor and the aromatic nucleotide bases, and this was confirmed in the case of the gas phase structure of the Zn–Sal–AMP anionic complex [13]. However, for similar Zn–salophen or Zn–salen adducts in solution it was reported [19, 20] that the interaction with diphosphate or ATP causes the demetallation of the metal complex with the formation of the free salophen ligand.

In light of all of these partially contrasting observations, we decided to perform a more in-depth investigation of the dynamics of the tetradentate Schiff base shown in Fig. 1a (Sal), its Zn(II) coordination compound (Zn–Sal, Fig. 1b) and the spectroscopic changes following the interaction between Zn–Sal and ADP in ethanol solutions, since the most relevant change in the luminescence properties were observed when Zn–Sal is associated with the ADP anion as a guest [17].

Furthermore, to gain information on the possible spatial and electronic structure of the Sal ligand, Zn–Sal and Zn–Sal–ADP, the complex system has been investigated by means of Density Functional Theory (DFT) and Time Dependent DFT (TD-DFT).

2 Experimental and theoretical procedures

2.1 Experimental section

The absorption spectra were recorded using an UV–Vis spectrophotometer (Jasco V-630) in the wavelength range from 250 to 600 nm. The spectra were recorded at room temperature from a solution of ethanol in fused silica cuvettes with an optical path length of 1 mm.

Sal and Zn–Sal was synthesized as described in previous investigations [17, 21]. ADP disodium salt was purchased from Sigma–Aldrich. Spectrophotometric grade ethanol was used as a solvent. To produce the Zn–Sal–ADP complex a saturated solution of ADP disodium salt in ethanol was used for the dilution of solid Zn–Sal.

The pump–probe experiments were performed using a laser system consisting of a 1 kHz, 4 mJ, 35 fs chirped pulse amplifier seeded by a Ti:Sa oscillator and the pump pulse was generated by an optical parametric amplifier. The experimental results reported in this work have been obtained with the pump wavelength set to 400 nm or to 330 nm. The probe was generated by focusing a small quantity of 800 nm light (1–3 μJ) into a rotating CaF_2 crystal and then collimating the white light supercontinuum generated. The optical layout of the commercial transient absorption spectrometer (Femto-Frame II, IB Photonics) consists of a split beam configuration in which 50% of the white light (350–800 nm) passes through the sample contained in a 1 mm static cell while the

remainder is used as a reference to account for pulse to pulse fluctuations in the white light generation. The pump pulse is focused (circular spot diameter = 400 µm) onto the sample with a power density of 150 µJ/cm^2. The probe pulse is much smaller (approximately 150 µm) and is delayed in time with respect to the pump by varying the length of its optical path. All experiments were performed with linear polarisation for both pump and probe pulses and the angle between the electric field vectors of the two was set to the magic angle to eliminate effects due to rotational dynamics. The instrument response function was measured to be approximately 70 fs. The set-up used for the transient absorption measurements has been described in detail elsewhere [22].

The fluorescence measurements were performed by exciting the samples using femtosecond pulsed radiation at 330 and 400 nm (1 kHz of repetition rate) focused to a diameter of approximately 50 µm, with an excitation density of about 50 mW/cm^2. The fluorescence spectra were collected using a monochromator (600 grooves/mm grating) coupled with a photomultiplier. The time-resolved measurements were performed with a time-correlated single photon counting (TCSPC) system with a photomultiplier as the detector with an instrumental response function (IRF) of 0.5 ns.

2.2 Theoretical section

The structures of Sal, Zn–Sal–EtOH have been optimized using the B3LYP/def2-TZVP method with BJ3 dispersion correction with the Orca package [23]. Given the large conformational flexibility of Zn–Sal–ADP, the possible geometries were explored by means of molecular dynamics (MD). In particular, a 25 ps MD trajectory was recorded using the DFTB + package [24] with SCC charges [25], dispersion interactions [26] and the 3ob parameter set. From the trajectory, a set of 200 structures were extracted. These structures were then optimized at the same DFTB level and we selected the seven with the lowest energy. These, in turn were optimized using B3LYP/def2-TZVP with BJ3 dispersion correction with the Orca package. Of these seven structures, we have selected four which turned out to be substantially different in conformation. The UV absorption spectra of the four Zn–Sal–ADP compounds, of Zn–Sal and of Sal, at their equilibrium geometries, have been computed using the g16 package [27] and the TD-DFT method with the B3LYP/6–311 + G(d,p) functional. The M06-2X functional has also been tested on the Zn–Sal system, but the agreement with the experimental absorption data deteriorates significantly with respect to B3LYP. The TD-DFT results reported here are based on requesting the first 15 singlet excited states and, to account for solvent effects, have been performed in ethanol using the PCM model. Interestingly, we did not find any extreme variation of the resulting UV absorption spectra between the four conformers of Zn–Sal–ADP, hence we shall use in the paper only two representants of it.

The optimizations of the geometries of the excited states have been computed with the TD-DFT gradient, calculated with the relaxed excited state density in ethanol (PCM model) as emerging from the B3LYP functional, but using a less computationally demanding double zeta basis set, the 6-31G(d).

3 Results and discussion

3.1 Steady state absorption spectra

In Fig. 2a, the absorption spectra of 3.5×10^{-5} M ethanol solutions of Sal (grey line), Zn–Sal (blue line) and Zn–Sal saturated with ADP (red and olive-green lines) in the 250–600 nm region are shown. The absorption spectrum

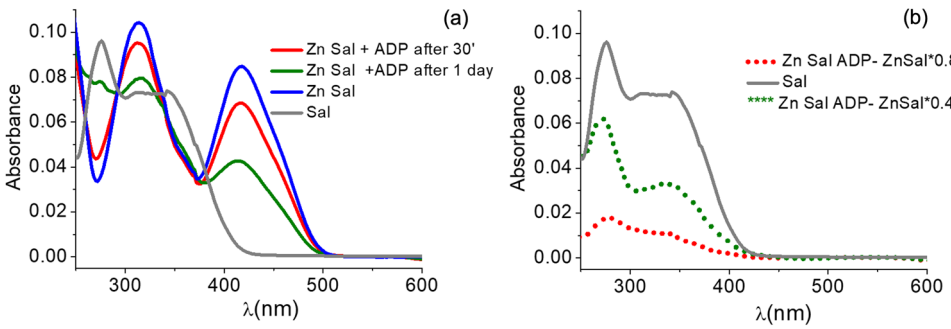

Fig. 2 **a** Steady state absorption spectra of 3.5×10^{-5} M ethanol solutions of Sal (grey line), Zn–Sal (blue line) and Zn–Sal saturated with ADP recorded 30 min after (red line) and 1 day after (olive-green line) the preparation of the sample. **b** Comparison between the absorption spectrum of an ethanol solution of salophen (grey line) and the difference spectra obtained by subtracting rescaled spectra of Zn–Sal from the spectra recorded for Zn–Sal ethanol solutions saturated with ADP. The red dotted line corresponds to the difference between the red spectrum in **a** minus the blue spectrum in **a** rescaled to 80% of its intensity. The olive-green dotted line corresponds to the difference between the olive-green spectrum in **a** minus the blue spectrum in **a** rescaled to 47% of its intensity. See text for details

of Zn–Sal in ethanol (blue line) displays bands centered at 314 and 420 nm while the ethanol solution of the Sal ligand (grey line) exhibits absorption bands centered at 274 and 330 nm. The spectrum of the freshly prepared Zn–Sal ethanol solution saturated with ADP, namely recorded 30 min after the preparation of the sample (Fig. 2a red line), showed negligible changes in shape of the absorption spectrum when compared to the spectrum of Zn–Sal (Fig. 2a blue line) in the 250–600 nm range. A decrease of about 20% of the absorption band at 420 nm (less pronounced for the other bands) with respect to the ethanol solution of Zn–Sal is ascertained. In Fig. 2a, the spectrum recorded one day after the preparation of the sample is also reported (olive-green line). In the latter case, we observe a decrease of about 53% of the absorption band at 420 nm with respect to the ethanol solution of Zn–Sal.

Assuming that the Zn–Sal solution saturated with ADP contains 80% (after 30 min) or 47% (after 1 day) of Zn–Sal not complexed with ADP, we rescaled the spectra of Zn–Sal to 80% or to 47% of their intensity and the rescaled spectra have been subtracted from the two spectra of the Zn–Sal solution saturated with ADP measured after 30 min and after 1 day accordingly. The result of the subtractions is reported in Fig. 2b as dotted lines, where the red dotted line is the outcome from the spectra measured after 30 min, while the olive-green dotted line is the outcome from the spectra measured after one day. The difference spectra strongly resemble the spectrum of the Sal ligand (shown for comparison in the same Fig. 2b, grey line), although the relative intensity of the absorption bands is not reproduced and a slight shift towards the blue of the band at 273 nm can be recognized. We, therefore, have the first indication that a demetallation process leading to the formation of the Sal ligand cannot be neglected. From the comparison of the absorption spectra we estimated that after 30 min about 7% of Sal is present in the solution and the percentage of Sal increases to 40% after one day. Therefore, the presence of a complex between Zn–Sal and ADP cannot be clearly inferred from the steady state absorption spectra, since the spectral modifications due to the addition of ADP to the Zn–Sal solution are only evident after the solution has been standing for some time and the observed differences in the absorption spectra can be attributed mostly to a demetallation process.

In Fig. 3a,b, the calculated oscillator strengths for selected vertical singlet−singlet transitions from the ground state (reported in Table S1 of the SI) for Sal and Zn–Sal–EtOH are shown and compared with their respective measured spectra in ethanol. Reasonable agreement is found between the experimental spectra and the computed transition for Sal and Zn–Sal–EtOH. In Fig. 3c, only the calculated oscillator strengths for two of the most stable predicted conformers of Zn–Sal–ADP are reported. The conformer *a* is a folded conformer, which is stabilized by π–π interactions between one salicylidene unit and adenine (see the structures in Fig. S1c of SI), while the conformer *b* has a T shaped conformation of adenine with respect to the aromatic ring of the salicylidene unit.

For both conformers strong absorption bands are predicted to be in the 315–360 and 400–450 nm range, as also found for Zn–Sal. In contrast, the lowest energy electronic transitions for the Sal ligand are centered well below 400 nm. From an inspection of the molecular orbitals, for all the species, the lowest energy excitations can be described as $\pi\pi^*$ transitions, as shown in Fig. S1 of SI.

3.2 Time-resolved absorption and fluorescence

Transient absorption spectra were recorded at pump–probe time delays between − 1 ps and 1 ns over the 400–750 nm spectral region following excitation either at 330 or at 400 nm. At 330 nm the absorption coefficient for the Sal is about 70% that of the absorption coefficient of Zn–Sal while at 400 nm the absorption coefficient for Sal is much lower (about 20% that of the absorption coefficient of Zn–Sal). We used solutions at a concentration in the range of 1–6 10^{-5} M for Zn–Sal in ethanol as well as for ethanol solutions saturated with ADP, to achieve adequate signal-to-noise ratios while preventing the formation of dimers. The concentration for the Sal ethanol solutions was 1.8×10^{-4} M due to the lower absorption coefficient of this species.

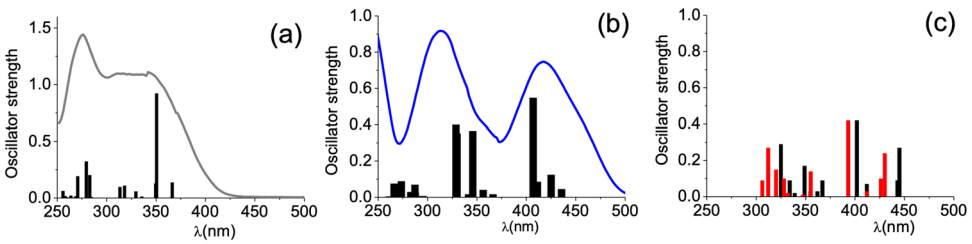

Fig. 3 TD-B3LYP/6–311 + G(d,p) calculated oscillator strengths (bars) of selected singlet−singlet transitions from S_0 compared with their respective experimental spectra in ethanol (lines) rescaled to assist comparison **a** Sal, **b** Zn–Sal–EtOH and **c** Zn–Sal–ADP (no comparison with experimental data). Oscillator strengths calculated for the two most stable conformers are reported as black lines for conformer *a* and red lines for conformer *b* (see Table S1 in SI)

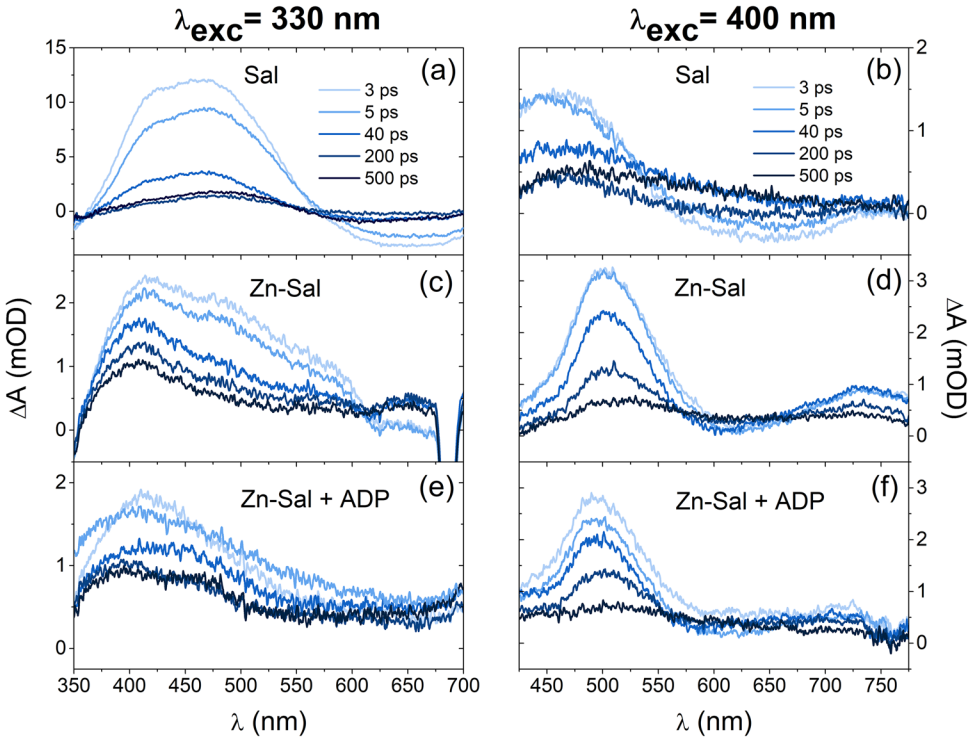

Fig. 4 Transient spectra at different time delays following laser excitation at 330 nm or 400 nm of ethanol solutions of Sal, Zn–Sal and freshly prepared Zn–Sal ethanol solution saturated with ADP. Probe wavelengths are 350–700 nm for excitation at 330 nm and 425–775 nm for excitation at 400 nm. **a** 1.8×10^{-4} M Sal in ethanol, $\lambda_{exc}=330$ nm; **b** 1.8×10^{-4} M Sal in ethanol, $\lambda_{exc}=400$ nm, pump energy 2.5 μJ **c** 2.3×10^{-5} M Zn–Sal in ethanol, $\lambda_{exc}=330$ nm; **d** 5.6×10^{-5} M Zn–Sal in ethanol, $\lambda_{exc}=400$ nm; **e** 1.4×10^{-5} M Zn–Sal in ethanol saturated with ADP, $\lambda_{exc}=330$ nm; **f** 1.4×10^{-5} M Zn–Sal in ethanol saturated with ADP, $\lambda_{exc}=400$ nm. Pump energy 1 μJ, except for Sal excited at 400 nm (**b**), where the pump energy was 2.5 μJ. Delay times are indicated in the legends

3.2.1 The uncoordinated salophen compound

Figure 4a, b shows the transient spectra at selected time delays for solutions of Sal in ethanol excited at 330 nm or at 400 nm. It can be seen that either by excitation at 330 nm (Fig. 4a) or at 400 nm (Fig. 4b) positive absorbance difference (ΔA) signals are measured in the 350–550 nm range, demonstrating a dominant contribution of excited state absorption bands, while negative ΔA signals are measured around 650 nm, which can be ascribed to stimulated emission. Ground state bleaching can be neglected around 650 nm, since salophen only absorbs at wavelengths below 450 nm (Fig. 2 grey line).

The temporal cuts for specific probe wavelengths intervals can be fit by a sum of exponential decays convolved with the instrumental function. The time constants with their relative amplitudes obtained from the best fits for selected and representative probe intervals are summarized in Table 1.

For the Sal ligand excited at 330 nm, the temporal behavior of the positive excited state absorption band centered around 460 nm can be fit with a mono exponential decay ($\tau_2=14\pm1$ ps in Table 1) plus a long-lived transient absorption contribution of the order of 9% that can be assigned to

Table 1 Time constants (τ_n) and relative amplitudes (A_n) obtained from the fits of the experimental temporal cuts for selected and representative probe wavelengths (λ_{probe})

	M (mol/l)	λ_{exc} (nm)	λ_{probe} (nm)	τ_1 (ps)	A_1 (%)	τ_2 (ps)	A_2 (%)	τ_3 (ps)	A_3 (%)
Sal	1.8×10^{-4}	330	460 ± 3			14 ± 1	91	> 1000	9
			640 ± 3			14 ± 1	− 100		
		400	455 ± 10	5 ± 3	31	27 ± 8	61	> 1000	8
			655 ± 10			26 ± 4	− 100		
Zn–Sal	2.3×10^{-5}	330	385 ± 5	0.4 ± 0.1	29	14 ± 1.6	28	> 1000	43
			505 ± 5	0.3 ± 0.03	62	12 ± 0.7	29	> 1000	8
	5.6×10^{-5}	400	500 ± 10	20 ± 3	24	203 ± 17	70	> 1000	6
			745 ± 20			206 ± 18	90	> 1000	10
Zn–Sal saturated with ADP (fresh solution)	1.4×10^{-5}	330	425 ± 5	0.7 ± 0.4	44	51 ± 15	50	> 1000	6
	$3.5\ 10^{-5}$ M	400	500 ± 10	3.6 ± 0.6	32	180 ± 18	55	> 1000	13

Pump wavelength (λ_{exc}) and solution concentrations (M) are specified

a very long decay process (> 1000 ps). Around 640 nm, the negative stimulated emission signal can be fit by a mono exponential recovery curve, characterized by a time constant $\tau_2 = 14 \pm 1$ ps. Thus, temporal evolution of both absorption and stimulated emission bands can be described by a time constant of ~ 14 ps. This strongly indicates that the same excited state is responsible for both signals, i.e. the positive signal is due to absorption from the excited state to higher lying states while the negative signal is due to stimulated emission from the same state. The measured time constant is comparable to the longest time constant obtained by fluorescence up-conversion measurements ($\tau = 14.8$ ps) [28] for an analogous salicylidene tetradentate Schiff base, excited at 385 nm in acetonitrile.

Similar results are found for excitation at 400 nm apart from an additional short decay time observed for the excited state absorption band. The small differences in the dynamics may be due to the fact that the first absorption maximum of Sal in solution is at 330 nm and, therefore, an excitation wavelength of 400 nm excites only the rising edge of the absorption maximum leading to a slightly different distribution of initially excited states. For excitation at 400 nm, the excited state absorption band centered around 460 nm (Fig. 4b) can be fit with a bi-exponential decay ($\tau_1 = 5 \pm 3$ ps, $\tau_2 = 27 \pm 8$ ps, Table 1) plus a residual transient absorption with a long lifetime. In the 600–800 nm range (Fig. 4b), the negative stimulated emission signal can be fit by a mono exponential recovery curve with a time constant $\tau_2 = 26 \pm 4$, as reported in Table 1.

3.2.2 The Zn–salophen complex

In Fig. 4c, d, the transient spectra at selected time delays for Zn–Sal ethanol solutions are shown. Figure 4c shows the transient spectra following excitation at 330 nm while Fig. 4d shows the transient spectra following excitation at 400 nm. The time constants obtained from the fits of the temporal cuts for selected probe wavelengths are summarized in Table 1.

For Zn–Sal ethanol solutions excited at 330 nm, Fig. 4c, positive ΔA signals are measured in the 375–550 nm range, which can be fit with two time constants of 0.3–0.4 ps and 12–15 ps plus a residual long-lived transient absorption contribution with a considerable amplitude only in the lower wavelength range (Table 1).

For excitation at 400 nm of Zn–Sal ethanol solutions, two excited state absorption bands are distinguishable in the transient spectra, centered around 500 nm and 745 nm. The temporal evolution of the bands can be fitted with time constants of 20 ± 3 ps and ~ 200 ps plus a residual long-lived transient absorption contribution as reported in Table 1. The residual long-lived contributions, found by excitation either at 330 nm or at 400 nm, can be associated with radiative relaxation. Indeed, we measured time-resolved fluorescence of a Zn–Sal ethanol solution excited at 400 nm or at 330 nm. For excitation at 400 nm the fluorescence emission is centered around 505 nm and presents a decay time constant of 2.3 ns (Fig. S2 of the SI). This result is in agreement with previous fluorescence measurements performed on Zn–Sal excited at 350 nm [17]. For excitation at 330 nm we observed two emission bands at 375 nm and at 490 nm, both with a shoulder (vibronic band) at 420 nm and 525 nm, respectively, as reported in Fig. S3 of the SI. The fluorescence decay is mono exponential for both bands with a lifetime of 5.3 ns for the emission band at 375 nm and of 1.8 ns for the emission band at 490 nm.

We assign the emission band at 375 nm to a highly fluorescent impurity and a probable candidate is 2,3-diaminonaphthalene [29] which was used for the synthesis of Sal. 2,3-diaminonaphthalene has an absorption coefficient at 330 nm, which is roughly a fifth of the absorption coefficient of Zn–Sal [21], and does not absorb for wavelengths higher than 380 nm. Therefore, while this impurity does not considerably influence the absorption and transient absorption measurements, it is clearly observed in the photoluminescence measurements due to its high fluorescence quantum yield (0.54) [30]. The reported fluorescence lifetime of 2,3-diaminonaphthalene of 5.7 ns, further supports our hypothesis [30].

3.2.3 Zn–Sal ethanol solution saturated with ADP

Figure 4 e,f shows the transient spectra at selected time delays for freshly prepared 1.4×10^{-5} Zn–Sal ethanol solutions saturated with ADP excited at 330 nm (Fig. 4e) or at 400 nm (Fig. 4f).

For excitation at 330 nm (Fig. 4e), clear differences can be noted in the 470–550 nm probe range from the transient spectra of the Zn–Sal ethanol solution (Fig. 4c). For instance, the transient spectrum taken at a 3 ps time delay of the ethanol solution of Zn–Sal (Fig. 4c) displays positive ΔA signals extending from 350 to 600 nm while the transient spectrum for the freshly prepared ethanol solution of Zn–Sal saturated with ADP (Fig. 4e) displays a narrower positive ΔA band centered around 425 nm. The temporal evolution of the latter mentioned band was fit with a bi-exponential decay ($\tau_1 = 0.7 \pm 0.4$ ps, $\tau_2 = 51 \pm 15$ ps, Table 1) plus a residual long-lived transient absorption contribution of the order of 6%. τ_2 (~ 51 ps) is substantially longer than the time constant measured for Zn–Sal (~ 13 ps, Table 1) and also longer than the time constant measured for the Sal ligand (~ 14 ps, Table 1) by excitation at 330 nm. These findings indicate the presence in the freshly prepared solution of a compound different from Sal or Zn–Sal that we assign to a complex between Zn–Sal and ADP.

The transient spectra for a freshly prepared 1.4×10^{-5} M Zn–Sal ethanol solution saturated with ADP and excited at 400 nm, Fig. 4f, showed negligible differences with respect to the transient spectrum of the 5.6×10^{-5} M Zn–Sal solution (Fig. 4d) in terms of the spectral response and time dependence (Table 1). We confirmed this result by measuring the transient spectra following excitation at 400 nm for solutions of Zn–Sal and Zn–Sal saturated with ADP at the same analytical concentration of Zn–Sal, as shown in Fig. S5a, b of SI. This finding indicates that the dynamics of Zn–Sal excited to its first absorption maxima at 400 nm is not significantly affected by the interaction with ADP.

The transient spectra were measured also after a few days for the ethanol solution of Zn–Sal saturated with ADP. For excitation at 330 nm, an excited state absorption band centered around 430 nm decays with time constants $\tau_1 = 0.4 \pm 0.1$, $\tau_2 = 15 \pm 2$ plus a long-lived transient absorption, values that are comparable to the decay time of Zn–Sal and Sal, though stimulated emission bands of Sal around 650 nm are not observed in these conditions. Similarly, for excitation at 400 nm of a solution that was standing a few days at room temperature, an excited state absorption band centered around 450 nm and a strong induced emission signal around 650 nm were observed (Fig. S5d in SI) greatly resembling the excited state absorption and stimulated emission bands of the Sal ligand solution (Fig. S5c in SI), in terms of the spectral response and time dependence.

These findings confirm that a slow demetallation of the complex takes place. In particular, the steady state absorption spectra and the transient absorption spectra of the Zn–Sal–ADP and Sal ethanol solutions confirm that after a few days the Zn^{2+} ion is almost fully displaced from the metal–ligand complex in the presence of ADP.

The fluorescence spectrum for excitation at 330 nm of a freshly prepared ethanol solution of Zn–Sal saturated with ADP is reported in Fig. S4 of the SI. Double fluorescence emission was observed also in this case. The spectrum resembles the spectrum of the Zn–Sal ethanol solution (Fig. S3 of the SI), although the blue shifted band, the band centered at 375 nm, is almost three times more intense with respect to the Zn–Sal ethanol solution at the same analytical concentration of Zn–Sal. The temporal evolution on the nanosecond time scale of both emission bands (Fig. S4 of the SI) is comparable to the temporal evolution observed for Zn–Sal ethanol solutions (Fig. S3 of the SI). Considering that this band can be attributed to the emission of 2,3-diaminonaphthalene, the latter finding indicates that the interaction with ADP leads not only to a displacement of Zn^{2+} from Zn–Sal, generating Sal, but also to a partial decomposition of Sal, into its molecular constituents, 2,3-diaminonaphthalene and 3-isopropylsalicylaldehyde.

The generation of 2,3-diaminonaphtalene and the detection of its fluorescence at 375 nm could be used as a probe for the detection of ADP. A similar strategy based on disassembly has been already proposed for zinc–salen complexes interacting with biologically relevant di- and tri-phosphates [19]. The approach was based on the turn on detection of the fluorescence around 500 nm of the salicylaldehyde produced from the disassembly of the complex. The advantage of using a Zn–salophen compound bearing a polycyclic naphthyl group is due to the fact that salicylaldehyde emission, besides having a lower quantum yield, is also partly superimposed on the Zn coordinated compounds fluorescence.

The ability of mono-, di- and tri-phosphates to selectively displace Zn^{2+} from Zn–salophen complexes analogues to Zn–Sal generating the free tetradentate Schiff base has been also previously reported [20, 31] and it was further shown that the demetallation process of a Zn–Sal complex into liposomes follows first order kinetics with time constants of the order of 1–3 days.

The process is presumably initiated by coordination of the diphosphates to the Zn atom, in line with previous experimental evidence [17, 19, 31]. Moreover, it is conceivable that the Zn ion is coordinated by the phosphate groups of ADP and ethanol molecules, since in water a stability constant of 5×10^4 is reported [32].

In agreement with a previous interpretation [20], we deduce that the multicharged phosphate anion of ADP favors the coordination of two Zn–Sal complexes to the nucleotide and this promotes the protonation of the phenolic positions initially coordinated to the Zn center leading to the formation of the demetallated Sal ligand which partially decomposes into its molecular constituents, one of which is highly fluorescent (2,3-diaminonaphthalene).

3.3 Interpretation of the observed electronic properties of Sal and Zn–Sal

The first absorption maximum of Sal in solution is at 330 nm and, therefore, 400 nm photons excite only the rising edge of the absorption. For the excitation of Sal at 330 and 400 nm we obtained substantially consistent results. The fact that ultrafast stimulated emission is observed in the 610–750 nm range for the Sal ligand points to a substantial drop of the energy gap between the lower-lying singlet excited state and the ground state, presumably caused by structural reorganization of the Sal ligand in its excited state. Relaxation occurs with a time constant which is longer at 400 nm ($\tau_2 \sim 26$ ps, Table 1) with respect to the constant obtained exciting at 330 nm ($\tau_2 \sim 14$ ps, Table 1). The absorption spectrum of Zn–Sal complex has two maxima at 314 and 420 nm, respectively. By excitation at 330 nm the Zn–Sal complex relaxes through fluorescence emission on a timescale of a few nanoseconds, as confirmed by time-resolved fluorescence measurements. In fact, the time constant of the residual long-lived transient absorption contribution, attributed to radiative

relaxation, is in agreement with the fluorescence measurements, while the shorter time constants ($\tau_1 = 0.3$–0.4 ps, $\tau_2 = 12$–15 ps, Table 1) can be related to internal conversion, vibrational relaxation, solvation processes and conformational motion. Solvation processes and vibrational relaxation are on the timescale of hundreds of femtoseconds to few picoseconds while conformational motion occurs on longer timescale [33]. Internal conversion can occur up to the nanosecond scale in these systems. Clearly these processes contribute in a different way to the overall relaxation which is difficult to disentangle. Furthermore, different excitation wavelengths can also result in different contributions of the four processes. By excitation at 400 nm, together with a time constant of a few picoseconds, we measured a time constant of ~ 200 ps and a residual long-lived transient contribution that fluorescence emission measurements confirmed to be a radiative relaxation on a nanosecond timescale.

These observations suggest that in the case of the Sal ligand both 330 and 400 nm radiation excite the same excited state possibly in different parts of the excited state surface leading to only minor differences in the dynamics. On the other hand, the dynamics of the Zn–Sal complex appears to vary quite significantly as a function of the excitation wavelength indicating the involvement of different excited states. These points are further discussed below in light of the theory results.

3.3.1 Excited state features of Sal, Zn–Sal–EtOH and Zn–Sal–ADP by TD-DFT calculations

The optimizations of the geometries of the most populated excited states have been computed with the TD-DFT gradient, at the less computationally demanding (B3LYP/6-31G(d) in ethanol) level of theory (Table S2 of the SI). Several bright states have been selected for Sal, Zn–Sal–EtOH and for two of the most stable calculated conformers of the 1:1 complex between Zn–Sal and ADP.

For Sal, the optimization of the excited state geometries of all the selected bright electronic states, produces always highly distorted geometries. A possible proton transfer from the oxygen to the nitrogen atom does not take place. The three bright states (S_1, S_3 and S_4) all originate from $\pi \rightarrow \pi^*$ transitions. The S_1 state arises from two dominant 1-electron excitations: $120 \rightarrow 121$ and $119 \rightarrow 122$ (where the HOMO is 120). The S_3 and S_4 states are two almost degenerate excited states arising from the 1-electron excitations: $119 \rightarrow 121$, $120 \rightarrow 122$ for S_3 and $119 \rightarrow 122$, $120 \rightarrow 121$ for S_4. By monitoring the electronic excitations, we have seen that during optimization, the $120 \rightarrow 121$ (HOMO-

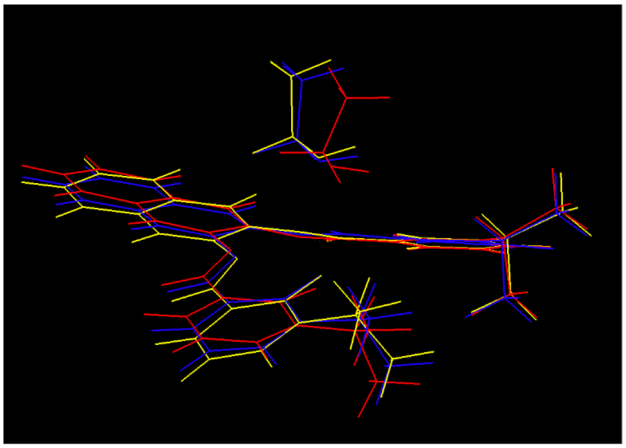

Fig. 6 S_0 (yellow), S_4 (red) and S_{10} (blue) minimum energy structures of Zn–Sal–EtOH in ethanol obtained at the TD-DFT-B3LYP/6-31G(d) level

LUMO) excitation quickly becomes the only dominant one. The same appear to happen for the S_4 state that is seen to cross the lower-lying state in few steps (Fig. 6, left) and become S_1. The S_3 state follows the same path as S_4. The relaxation of the S_3 and S_4 excited states due to the mixing and crossing quickly transforms them into the first excited state of the system (S_1). Figure 5a reports the optimized geometry for the S_0 ground state of Sal and, as an example, the S_4 optimized structure. It can be seen in Fig. 5b that the energy of the S_4 optimized geometry falls to only 0.67 eV above the S_0 energy of the ground state geometry set as the zero-point of the energy scale, with an energy loss of 2.9 eV. Similar results have been found for S_1 and S_3 optimizations (Table S2 of the SI). Therefore, we infer that the relaxation of Sal is mainly associated with torsional motion, as previously pointed out [28, 34, 35]. The experimental

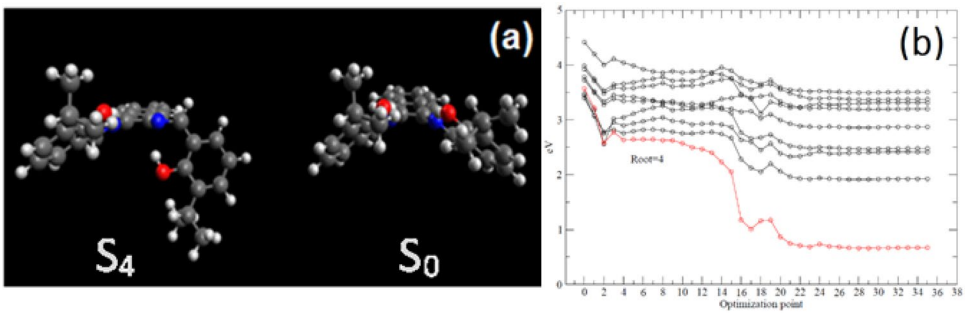

Fig. 5 **a** Ground and S_4 excited states optimized structures of Sal; **b** S_4 excited state optimization (red line) with the other lowest singlet electronic excited states (black lines). The energy is referred to the equilibrium geometry of the electronic ground state

results suggest that the system relaxes by conformational adjustment on a timescale of ~ 15–30 ps, depending on the excess energy furnished by the photon. The observed positive residual long living (> 1 ns, Table 1) transient absorption signal can be associated with induced absorption from a non-radiative state, although we cannot exclude that, in the case of Sal ligand, it could be associated with an impurity, as found for an analogous salicylidene tetradentate Schiff base [28].

Figure 6 shows the comparison between the S_0 ground state geometry of Zn–Sal–EtOH and the structures obtained by optimization of the geometry of the bright electronic states around 409 nm (state S_4 Table S2 of the SI) and 329 nm (state S_{10} Table S2 of the SI). The structure obtained by geometry optimization of the S_9 bright state is almost equivalent to that obtained by optimization of S_{10}. It can be noticed that, in contrast to what is found in the case of the Sal ligand, the geometry changes with respect to the minimum energy structure of S_0 are minimal.

In Fig. 7, the excited state energy profiles of Zn–Sal–EtOH, obtained for the S_4 (a), S_9 (b) and S_{10} (c) excited states optimization, are shown. The three bright states S_4, S_9 and S_{10} essentially originate from $\pi \rightarrow \pi^*$ transitions (see Fig. S1 of the SI) in an analogous fashion to what we have seen for Sal. The S_4 state is dominated by $146 \rightarrow 148$ and $147 \rightarrow 149$ 1-electron transitions (where 147 is the HOMO). The other two present a larger number of 1-electron contributions, the largest being $144 \rightarrow 149$ for S_9 and $143 \rightarrow 149$ for S_{10}. During optimization, S_4 quickly crosses with the low-lying states, becomes S_1 and evolves accordingly (Fig. 7, left). S_9 and S_{10} are strongly mixed with each other, but while the former quickly becomes dominated by a $144 \rightarrow 148$ excitation and does not lower its energy, the latter crosses several states, lowers significantly its energy and becomes a low-lying excited state ($147 \rightarrow 149$). For S_4 optimization, the energy of the optimized geometry falls from 3.1 to 2.2 eV above the S_0 energy of the ground state geometry set as the zero-point of the energy scale. The resulting oscillator strength for the S_4 excited state relaxed geometry is, however, very low ($f = 0.02$, Table S2 of the SI). Although nanosecond lasting emission from similar salicylidene compounds has been questioned [28, 35, 36], we observed fluorescence emission centered at 505 nm by excitation at 400 nm of the Zn–Sal–ethanol solution, and we associate the residual transient absorption signal observed on a timescale longer than 1 ns to the radiative relaxation from a low-lying singlet excited state to the ground state. A possible impurity contribution was excluded because it does not absorb significantly at wavelengths longer than 380 nm.

For excitation at 330 nm two bright states, S_9 and S_{10}, with similar energy, are populated. For S_9 and S_{10} optimization (Fig. 7b and c), the energy of the optimized geometry falls, respectively, from 3.8 to 3.3 eV and from 3.8 eV to 2.7 eV above the S_0 energy of the ground state geometry set as the zero-point of the energy scale. In both cases, the resulting oscillator strengths are appreciable ($f = 0.6$–0.9, Table S2 of SI).

For the Zn–Sal–ADP complex, we carried out only a preliminary theoretical investigation assuming the presence, in a freshly prepared solution of a 1:1 adduct between Zn–Sal and ADP, since a theoretical investigation of complexes containing two Zn–Sal units is computationally too demanding at the present time. The TG-B3LYP/6-31G(d) optimization of the bright states around 400 nm (S_1, S_4) or at higher energy (S_{10}–S_{15}) of the Zn–Sal–ADP complex, as reported in Table S2 of the SI, leads to different results for the two investigated conformers. For conformer b, the theoretical outcome is analogous to what is found for Zn–Sal, and in fact the resulting oscillator strengths following excitation around 320–350 nm are not negligible. On the other hand, the oscillator strength predicted for conformer a is very low for excitation around 320–350 nm, suggesting the absence of fluorescence emission.

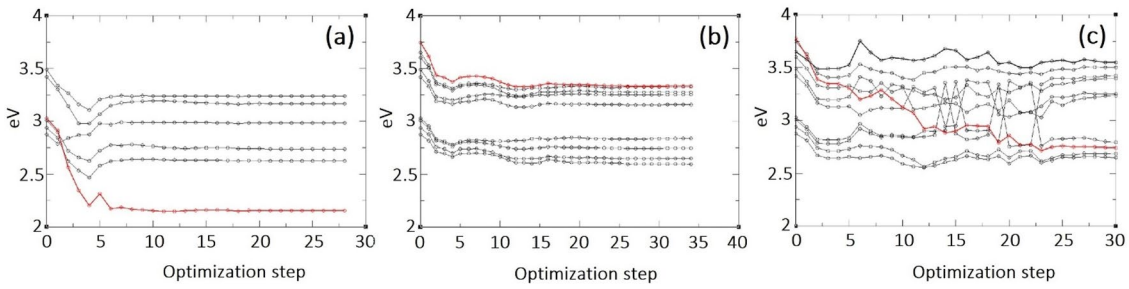

Fig. 7 S_4 (**a**), S_9 (**b**) and S_{10} (**c**) excited states optimization of Zn–Sal–EtOH (red lines). The other singlet electronic excited states are shown in black. The energy is referred to the equilibrium geometry of the electronic ground state

4 Conclusions

The dynamics of the Sal ligand, its Zn–Sal metal complex and the spectroscopic changes following the interaction between Zn–Sal and ADP in ethanol solution were investigated by steady state UV–Vis, ultrafast transient absorption and fluorescence emission spectroscopies. DFT and TD-DFT calculations assisted in the interpretation of the experimental results.

The deactivation of the excited state of Sal occurs through torsional motion, thanks to its rotatable bonds and twistable angles with a time constant for the relaxation of the order of a few tens of picoseconds. Complexation with Zn(II) causes rigidification of Sal structure, causing minimal geometry changes between the excited and ground states. Following conformational reorganization, the system relaxes radiatively on a timescale of a few nanoseconds.

By addition of ADP to a freshly prepared Zn–Sal ethanol solution, the static absorption properties of Zn–Sal are not distinctly altered, and the transient absorption spectra measured at 400 nm shows negligible differences. On the other hand, we measured a longer relaxation constant in the transient absorption spectra by excitation at 330 nm, in comparison with Sal and Zn–Sal and assign it to the presence, in a freshly prepared solution, of an unstable complex of Zn–Sal and ADP.

After a few days, however, the solution displayed the same static and kinetic behavior of a solution containing only the Sal ligand, indicating that the coordination of the diphosphate anion with the Zn atom leads to the demetallation of the Zn–Sal complex. This process is, therefore, the principal reason for the significant variations in the static absorption spectra and fluorescence emission around 500 nm observed following the addition of ADP to the Zn–Sal solution, in contrast with previously reported results.

Moreover, the ADP–Zn–Sal ethanol solution displayed an enhanced fluorescence at 375 nm, which we attribute to the 2,3-diaminonaphthalene formed by the decomposition of the Sal ligand and already present as an impurity in the Zn–Sal solution. Even if 2,3-diaminonaphthalene is formed in exiguous quantities, it is highly fluorescent and could function as a probe for the detection of ADP, since the interaction between Zn–Sal and ADP leads to the decomposition of the complex and to the formation of 2,3-diaminonaphtalene, whose fluorescence can be selectively detected at 375 nm.

Supplementary Information The online version contains supplementary material available at https://doi.org/10.1007/s43630-021-00165-0.

Acknowledgements A.D.C. acknowledges Sapienza Progetti di Ateneo 2017.

Declarations

Conflict of interest On behalf of all authors, the corresponding author states that there is no conflict of interest.

References

1. Pfeiffer, P., Breith, E., Lübbe, E., & Tsumaki, T. (1933). Tricyclische orthokondensierte Nebenvalenzringe. *European Journal of Organic Chemistry, 503*, 84–130. https://doi.org/10.1002/jlac.19335030106
2. Vigato, P. A., & Tamburini, S. (2004). The challenge of cyclic and acyclic Schiff bases and related derivatives. *Coordination Chemistry Reviews, 248*, 1717–2128. https://doi.org/10.1016/j.cct.2003.09.003
3. Erxleben, A. (2018). Transition metal salen complexes in bioinorganic and medicinal chemistry. *Inorganica Chimica Acta, 472*, 40–57. https://doi.org/10.1016/j.ica.2017.06.060
4. Pessoa, J. C., & Correia, I. (2019). Salan vs. salen metal complexes in catalysis and medicinal applications: Virtues and pitfalls. *Coordination Chemistry Reviews, 388*, 227–247. https://doi.org/10.1016/j.ccr.2019.02.035
5. Zhang, J., Xu, L., & Wong, W.-Y. (2018). Energy materials based on metal Schiff base complexes. *Coordination Chemistry Reviews, 355*, 180–198. https://doi.org/10.1016/j.ccr.2017.08.007
6. Brabec, V., Hrabina, O., & Kasparkova, J. (2017). Cytotoxic platinum coordination compounds. DNA binding agents. *Coordination Chemistry Reviews, 351*, 2–31. https://doi.org/10.1016/j.ccr.2017.04.013
7. Leoni, L., Carletta, A., Fusaro, L., Dubois, J., Tumanov, N. A., Aprile, C., Wouters, J., & Dalla Cort, A. (2019). A simple and efficient mechanochemical route for the synthesis of salophen ligands and of the corresponding Zn, Ni, and Pd complexes. *Molecules, 24*(12), 2314. https://doi.org/10.3390/molecules24122314
8. Oliveri, I. P., Malandrino, G., & Di Bella, S. (2014). Self-assembled nanostructures of amphiphilic zinc(II) salophen complexes: role of the solvent on their structure and morphology. *Dalton Transactions, 43*, 10208–10214. https://doi.org/10.1039/C4DT00973H
9. Consiglio, G., Failla, S., Oliveri, I. P., Purrello, R., & Di Bella, S. (2009). Controlling the molecular aggregation. An amphiphilic Schiff-base zinc(II) complex as supramolecular fluorescent probe. *Dalton Transactions, 47*, 10426–10428. https://doi.org/10.1039/B914930A
10. Yin, H.-Y., & Tang, J. (2017). Introducing metallosalens into biological studies: The renaissance of traditional coordination complexes. *European Journal of Inorganic Chemistry, 44*, 5085–5093. https://doi.org/10.1002/ejic.201700695
11. Germain, M. E., Thomas, R., Vargo, T. R., Khalifah, P. G., & Knapp, M. J. (2007). Fluorescent detection of nitroaromatics and

2,3-Dimethyl-2,3-dinitrobutane (DMNB) by a zinc complex: (salophen)Zn. *Inorganic Chemistry, 46*(11), 4422–4429. https://doi.org/10.1021/ic062012c
12. Consiglio, G., Oliveri, I. P., Failla, S., & Di Bella, S. (2019). On the aggregation and sensing properties of zinc(II) Schiff-base complexes of salen-type ligands. *Molecules, 24*(13), 2514. https://doi.org/10.3390/molecules24132514
13. Ciavardini, A., Dalla Cort, A., Fornarini, S., Scuderi, D., Giardini, A., Forte, G., Bodo, E., & Piccirillo, S. (2017). Adenosine monophosphate recognition by zinc–salophen complexes: IRMPD spectroscopy and quantum modeling study. *Journal of Molecular Spectroscopy, 335*, 108–116. https://doi.org/10.1016/j.jms.2017.02.014
14. Ciavardini, A., Fornarini, S., Dalla Cort, A., Piccirillo, S., Scuderi, D., & Bodo, E. (2017). Experimental and computational investigation of salophen-Zn gas phase complexes with cations: A source of possible interference in anionic recognition. *Journal of Physical Chemistry A, 121*(37), 7042–7050. https://doi.org/10.1021/acs.jpca.7b05825
15. Wezenberg, S. J., Escudero-Adan, E. C., Benet-Buchholz, J., & Kleij, A. W. (2009). Anion-templated formation of supramolecular multinuclear assemblies. *Chemistry, 15*, 5695–5700. https://doi.org/10.1002/chem.200900528
16. Dalla Cort, A., De Bernardin, P., & Schiaffino, L. (2009). A new water soluble Zn-salophen derivative as a receptor for α-aminoacids: Unexpected chiral discrimination. *Chirality, 21*, 104–109. https://doi.org/10.1002/chir.20614
17. Cano, M., Rodrıguez, L., Lima, J. C., Pina, F., Dalla Cort, A., Pasquini, C., & Schiaffino, L. (2009). Specific supramolecular interactions between Zn^{2+}-salophen complexes and biologically relevant anions. *Inorganic Chemistry*. https://doi.org/10.1021/ic900557n
18. Piccinno, M., Aragay, G., Yafteh Mihan, F., Ballester, P., & Dalla Cort, A. (2015). Unexpected emission properties of a 1,8-naphthalimide unit covalently appended to a Zn–salophen. *European Journal of Inorganic Chemistry*. https://doi.org/10.1002/ejic.201500258
19. Kumari, N., & Zelder, F. (2015). Detecting biologically relevant phosphates with locked salicylaldehyde probes in water. *Chemical Communnications, 51*, 17170. https://doi.org/10.1039/C5CC07413D
20. Wezenberg, S. J., Anselmo, D., Escudero-Adán, E. C., Benet-Buchholz, J., & Kleij, A. W. (2010). Dimetallic activation of dihydrogen phosphate by Zn(salphen) chromophores. *European Journal of Inorganic Chemistry, 29*, 4611–4616. https://doi.org/10.1002/ejic.201000455
21. Dalla Cort, A., Mandolini, L., Pasquini, C., Rissanen, K., Russo, L., & Schiaffino, L. (2007). Zinc–salophen complexes as selective receptors for tertiary amines. *New Journal of Chemistry, 31*, 1633–1638. https://doi.org/10.1039/B700723J
22. Catone, D., Di Mario, L., Martelli, F., O'Keeffe, P., Paladini, A., Pelli Cresi, J. S., Sivan, A. K., Tian, L., Toschi, F., & Turchini, S. (2020). Ultrafast optical spectroscopy of semiconducting and plasmonic nanostructures and their hybrids. *Nanotechnology, 32*(2), 025703. https://doi.org/10.1088/1361-6528/abb907
23. Neese, F. (2018). Software update: The ORCA program system, version 4.0. *Wiley Interdisciplinary Reviews, 8*, 1. https://doi.org/10.1002/wcms.1327
24. Aradi, B., Hourahine, B., & Frauenheim, T. (2007). DFTB+, a sparse matrix-based implementation of the DFTB method. *Journal of Physical Chemistry A, 111*, 5678–5684. https://doi.org/10.1021/jp070186p
25. Elstner, M., Porezag, D., Jungnickel, G., Elsner, J., Haugk, M., Frauenheim, T., Suhai, S., & Seifert, G. (1998). Self-consistent-charge density-functional tight-binding method for simulations of complex materials properties. *Physical Review B, 58*, 7260–7268. https://doi.org/10.1103/PhysRevB.58.7260
26. Elstner, M., Hobza, P., Frauenheim, T., Suhai, S., & Kaxiras, E. (2001). Hydrogen bonding and stacking interactions of nucleic acid base pairs: A density-functional-theory based treatment. *The Journal of Chemical Physics, 114*, 5149–5155. https://doi.org/10.1063/1.1329889
27. Frisch, M. J., Trucks, J. W., Schlegel, H. B., Scuseria, G. E., Robb, M. A., Cheeseman, J. R., Scalmani, G., Barone, V., Petersson, G., Nakatsuji, H., et al. (2016). *Gaussian 16, revision A.03*. Gaussian, Inc.
28. Khan, T., Vaidya, S., Mhatre, D. S., & Datta, A. (2016). The prospect of salophen in fluorescence lifetime sensing of Al^{3+}. *The Journal of Physical Chemistry B, 120*, 10319–10326. https://doi.org/10.1021/acs.jpcb.6b05854
29. Taniguchi, M., & Lindsey, J. S. (2018). Database of absorption and fluorescence spectra of >300 common compounds for use in photochemCAD. *Photochemistry and Photobiology, 94*, 290–327. https://doi.org/10.1111/php.12860
30. Manoharan, R., & Dogra, S. K. (1988). Acidity constants in the excited states: Absence of an excited-state prototropic equilibrium for the monocation–neutral pair of 2,3-diaminonaphthalene. *Journal of Physical Chemistry, 92*, 5282–5287. https://doi.org/10.1021/j100329a043
31. Gasbarri, C., Angelini, G., Fontana, A., De Maria, P., Siani, G., Giannicchi, I., & Dalla Cort, A. (2012). Kinetics of demetallation of a zinc–salophen complex into liposomes. *Biochimica et Biophysica Acta, 1818*, 747–752. https://doi.org/10.1016/j.bbamem.2011.10.014
32. Sayer, A. H., Blum, E., Major, D. T., Vardi-Kilshtain, A., Levi Hevroni, B., & Fischer, B. (2015). Adenosine/guanosine-3',5'-bis-phosphates as biocompatible and selective Zn2+ ion chelators. Characterization and comparison with adenosine/guanosine-5'-di-phosphate. *Dalton Transactions, 44*, 7305. https://doi.org/10.1039/C5DT00080G
33. Dobryakov, A. L., Kovalenko, S. A., & Ernsting, N. P. (2005). Coherent and sequential contributions to femtosecond transient absorption spectra of a rhodamine dye in solution. *The Journal of Chemical Physics, 123*(4), 044502. https://doi.org/10.1063/1.1948383
34. Vivas, M. G., Germino, J. C., Barboza, C. A., Vazquez, P. A. M., De Boni, L., Atvars, T. D. Z., & Mendonça, C. R. (2016). Excited-state and two-photon absorption in salicylidene molecules: The role of Zn(II) planarization. *Journal of Physical Chemistry C, 120*, 4032–4039. https://doi.org/10.1021/acs.jpcc.5b12042
35. Barboza, C. A., Germino, J. C., Santana, A. M., Quites, F. J., Vazquez, P. A. M., & Atvars, T. D. Z. (2015). Structural correlations between luminescent properties and excited state internal proton transfer in some Zinc(II) N, N′-Bis(salicylidenes). *Journal of Physical Chemistry C, 119*, 6152–6163. https://doi.org/10.1021/jp510476h
36. Gondia, N. K., & Sharma, S. K. (2019). Comparative optical studies of naphthalene based Schiff base complexes for colour tunable application. *Materials Chemistry and Physics, 224*, 314–319. https://doi.org/10.1016/j.matchemphys.2018.12.014

Authors and Affiliations

Patrick O'Keeffe[1] · Daniele Catone[2] · Stefano Turchini[2] · Alessandra Paladini[1] · Antonella Dalla Cort[3] · Enrico Bodo[3] · Susanna Piccirillo[2,4]

[1] Istituto di Struttura della Materia-CNR (ISM-CNR), EuroFEL Support Laboratory (EFSL), 00015 Monterotondo Scalo, Italy

[2] Istituto di Struttura della Materia-CNR (ISM-CNR), EuroFEL Support Laboratory (EFSL), Via del Fosso del Cavaliere 100, 00133 Rome, Italy

[3] Dipartimento di Chimica, Università di Roma "La Sapienza", Rome, Italy

[4] Dipartimento di Scienze e Tecnologie Chimiche, Università di Roma "Tor Vergata", Rome, Italy